THE JOURNAL OF PHYSICAL CHEMISTRY LETTERS
A JOURNAL OF THE AMERICAN CHEMICAL SOCIETY

pubs.acs.org/JPCL

Letter

Unraveling Ion Migration Mechanisms under Operating Conditions in Perovskite Solar Cells by Variable-Load Transient Photoelectric Technique

Yiyi Li,[▽] Shujie Qu,[▽] Jiyuan Wu, Haohui Fang, Ning Liu, Peng Cui, Meicheng Li,* and Xicheng Ai*

Cite This: *J. Phys. Chem. Lett.* 2024, 15, 11903−11910

Read Online

ACCESS | Metrics & More | Article Recommendations | Supporting Information

ABSTRACT: Ion migration in perovskite solar cells (PSCs) significantly impacts their photoelectric performance and physicochemical stability. Existing research has predominantly focused on inhibiting ion migration through chemical strategies or observing it under open-circuit or short-circuit conditions. This focus has led to a limited theoretical understanding and control of ion migration under practical conditions, constraining advances in long-term stability. In this study, we introduce a novel variable-load transient photoelectric technique (VL-TPT) to investigate ion migration dynamics in PSCs under practical operating conditions. Results show that ion accumulation correlates with photogenerated carrier concentration under open-circuit conditions. During operation, ion accumulation decreases with reduced load, because charge is transferred to the external circuit, leading to a reduction in carrier concentration within the device. An unusual increase in interface ions is observed at low loads due to interactions between charges accumulated in the potential well and ions. Introducing FA^+ in $MA_{0.75}FA_{0.25}PbI_3$ devices suppresses ion migration in the open-circuit state but accelerates interface ion buildup under operating conditions. These findings provide valuable insights for enhancing device stability and performance.

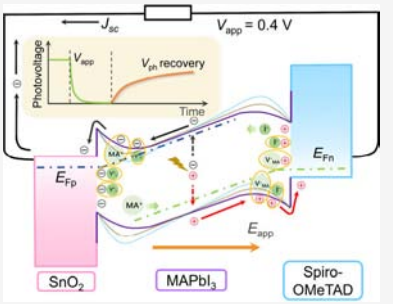

Over the past decades, organic−inorganic hybrid metal halide perovskite solar cells (PSCs) have garnered significant attention, with power conversion efficiency rapidly increasing from 3.8% to 26.7%.[1,2] This interest stems from their exceptional optoelectronic properties, including long free carrier lifetimes, excellent charge carrier diffusion lengths, and low defect state densities.[3−5] However, ion migration severely impacts the operational stability of PSCs, limiting their practical application. Ion migration refers to the movement and redistribution of ions within PSCs under external stresses such as light, heat, or electric fields, leading to current−voltage (J−V) hysteresis[6] and unstable power output.[7,8]

Current research focuses on chemical strategies to suppress ion migration, including perovskite compositional engineering, ligand engineering, additive engineering, and perovskite/charge transport layer interface engineering.[9,10] Doping pure methylammonium perovskite with formamidinium or cesium ions raises the ion migration barrier, thereby reducing ion migration.[9] Additives like lead thiocyanate increase perovskite crystal size and decrease grain boundaries, thereby reducing the number of migrating ions.[11] Modifying the perovskite/electron transport layer interface with fullerene derivatives passivates both anionic and cationic defects, lessening the impact of ion migration on device performance.[10,12] Despite these advances, methods remain empirical, lacking a systematic theoretical foundation and clear guidelines for controlling ion migration to improve long-term device stability.

An in-depth understanding of ion dynamics in PSCs is essential and witnessed notably advancements in recent years for interpreting their operational mechanisms and optimizing their performance, yet the intricacies of ion migration mechanisms under practical operating conditions remain elusive.[6,13−18] Most studies on photoelectric conversion mechanisms focus on extreme conditions, such as "open-circuit" or "short-circuit" states, where the device outputs no power.[19] Current methods for assessing steady-state efficiency, which utilizes continuous illumination and extended bias to mimic operating conditions,[19−21] may not accurately represent the true carrier and ion dynamics observed under practical operating conditions, such as those involving variable loads and illumination. Moreover, several methods are available to explore and characterize ion migration, including time-of-flight mass spectrometry,[22,23] photoluminescence microscopy,[24] and electrochemical impedance spectroscopy.[6,18,25,26] However, the overlapping ion migration processes with different time scales (e.g., iodide ions on the microsecond scale, methylammonium ions on the second scale)[27,28] and multiple photoelectric conversion processes[17] (e.g., charge transfer and recombination) complicate the

Received: October 24, 2024
Revised: November 16, 2024
Accepted: November 19, 2024
Published: November 21, 2024

ACS Publications

© 2024 American Chemical Society

https://doi.org/10.1021/acs.jpclett.4c03068
J. Phys. Chem. Lett. 2024, 15, 11903−11910

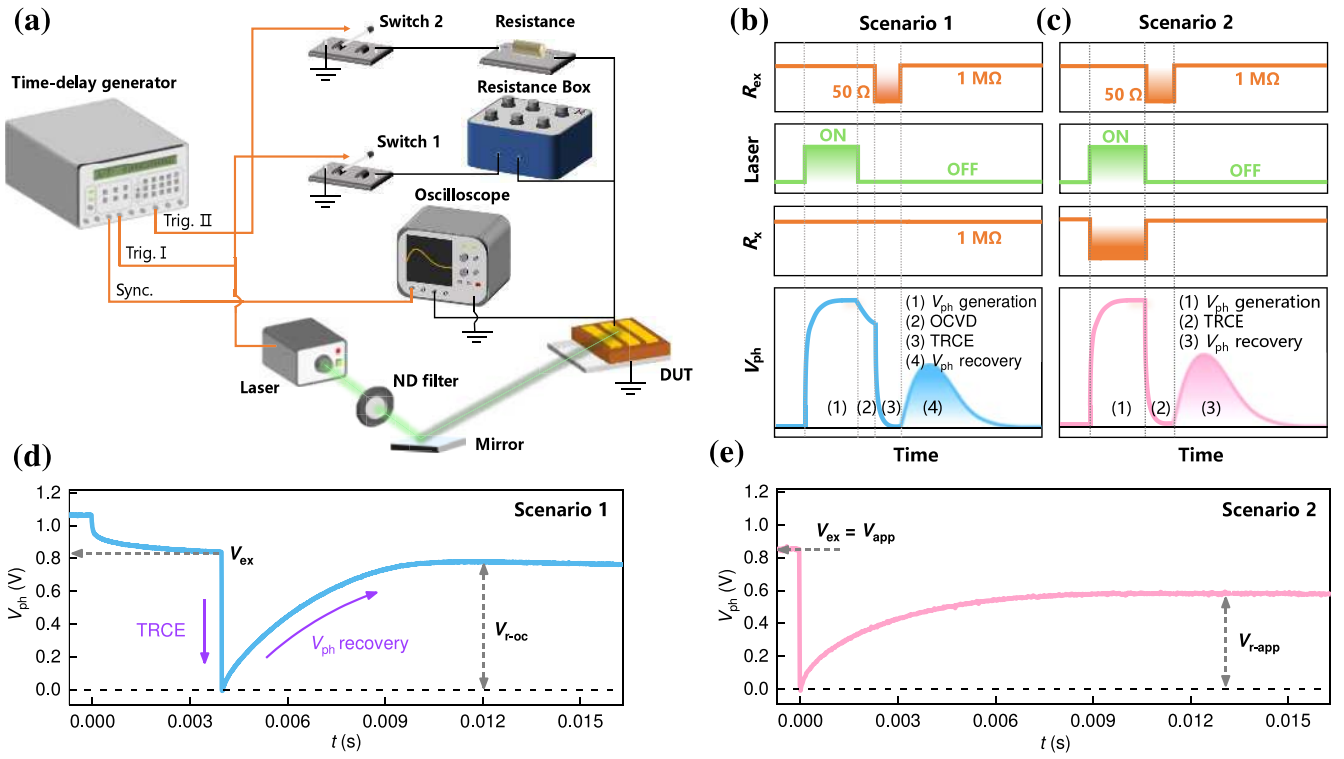

Figure 1. (a) Schematic illustration of the VL-TPT setup. Representative time sequences of the VL-TPT experiment working in the variable time delay mode (b) and the fluctuating load mode (c). (d, e) Exemplary VL-TPT profile of PSCs in the variable time delay mode (panel (d)) and the fluctuating load mode (panel (e)).

analysis of ion migration mechanisms under operating conditions. Therefore, research into ion migration dynamics across a broad time domain, with differentiation of ion types, is crucial for understanding ion-carrier interactions and improving long-term device performance.

Herein, we successfully distinguished the signals of free carriers from those of ion-related carriers under operating conditions utilizing the newly developed variable-load transient photoelectric technique (VL-TPT). Under operating conditions, the working electric field decreases interfacial carrier concentration by driving charge transfer to the external circuit, which reduces accumulated ions. Simultaneously, charges accumulated in the interfacial potential well attract additional ions to the interface. The introduction of FA^+ suppresses overall ion migration under open-circuit conditions, leading to increased ion accumulation.

To investigate ion migration mechanisms in PSCs under operating conditions, we employed a custom VL-TPT for quantitative analysis. This technique evolved from the circuit-switched transient photoelectric technique (cs-TPT) used in previous work,[29] with experimental details provided in the experimental section. As illustrated in Figure 1a, the photovoltaic device is connected in parallel with a CMOS switch and an oscilloscope. The time sequence of the VL-TPT system is controlled by a time delay generator, enabling rapid switching between the "short-circuit" state and "open-circuit" state/operating conditions. Based on the above setup, the VL-TPT experiment can be conducted in variable time delay mode and fluctuating load mode (Figures 1b and 1c), which are used to investigate ion migration in the device under open-circuit and operating conditions, respectively.

As the device is under variable time delay modes (under "open-circuit" state), the dynamics process consists of four steps (Figure 1b):

(1) The device is continuously illuminated until photogenerated voltage (V_{ph}) reaches its maximum.

(2) After removing the illumination, V_{ph} decay is recorded in real time, similar to open-circuit voltage decay (OCVD) measurements.

(3) At a specific time delay in the OCVD process, the circuit switches from an "open-circuit" to a "short-circuit" state, resulting in a sudden drop in V_{ph}. In this process, all free photogenerated carriers will be extracted to the external circuit.

(4) When the circuit switches back to an "open-circuit" state, a peculiar V_{ph} recovery phenomenon is revealed, as a distinctive feature of the VL-TPT curve.

In previous work, the V_{ph} recovery signal was attributed to the polarization-induced trap state model (PITS, see ref 26 and Figure S1), where photogenerated carriers trapped by ions accumulated at the interface are released and transferred to the charge transport layer. Therefore, the peak of the voltage recovery signal can reflect the amount of ion accumulation at the interface. This model has been utilized to investigate ion migration across different crystal facets,[30] evaluate the effects of NH_4PF_6-treated fluorine-doped tin oxide (FTO) substrates on ion migration,[31] and analyze how ion migration impacts hysteresis.[32]

On the other hand, as the device is under operating conditions with fluctuating load mode and at the same time delay (0 s), the dynamic process consists of three steps (Figure 1c):

https://doi.org/10.1021/acs.jpclett.4c03068
J. Phys. Chem. Lett. 2024, 15, 11903−11910

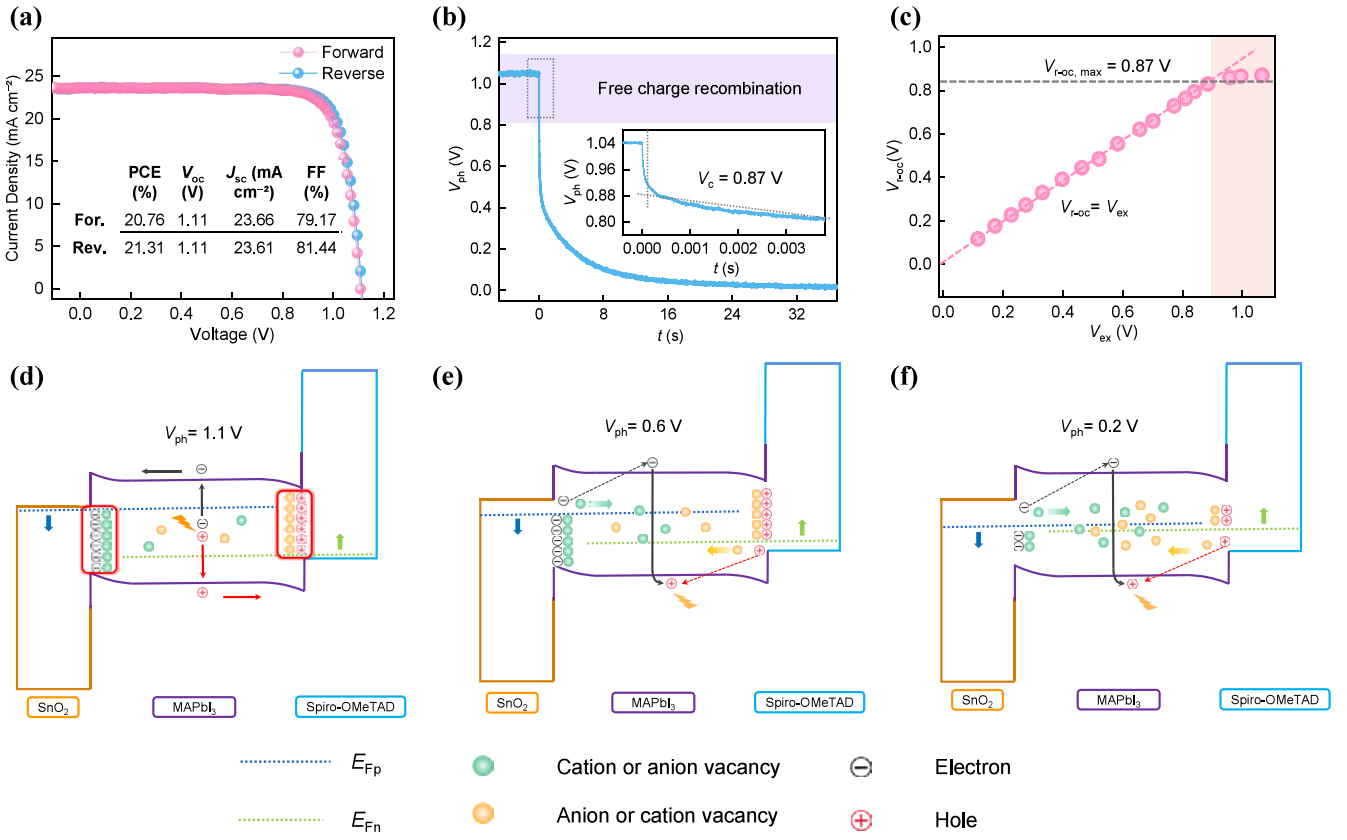

Figure 2. (a) The $J-V$ curves of the $MAPbI_3$ device. (b) The OCVD profile of the $MAPbI_3$ device. Inset: a zoomed-in scale of OCVD kinetics of the device within the first 4 ms, showing that the steep decay changes to the gradual one at V_c = 0.87 V (see the text for details). (c) $V_{r\text{-}oc}$ variation as a function of V_{ex} for the $MAPbI_3$ device. $V_{r\text{-}oc}$ increases linearly and then saturates at 0.87 V. (d)-(f) The energy band structure of the $MAPbI_3$ device under an "open-circuit" state at photovoltage (V_{ph}) values of 1.1 V (d), 0.6 V (e), and 0.2 V (f), respectively. As charge recombination occurs, the voltage decreases and the quantity of ions accumulated at the surface reduces.

(1) The device is illuminated while a load is connected across its terminals, with the load size adjusted to change the final stable operating voltage (V_{app}).

(2) When switching from operating conditions to "short-circuit" states and removing the illumination and load, a rapid decay of the voltage is observed due to free charge extraction.

(3) After returning to the "open-circuit" state, the VL-TPT dynamics are measured under different loads.

Beyond the upright configuration explored in this work, this approach is considered applicable for investigating ion migration dynamics in other perovskite solar cell structures, including inverted and dye-sensitized devices. Moreover, comparative experiments (Figure S2) on silicon-based solar cells with no ion migration (showing no voltage recovery) and dye-sensitized solar cells with ion migration (showing voltage recovery), further validate the general applicability of our method for studying ion migration dynamics in diverse devices.

Figures 1d and 1e display typical experimental VL-TPT curves for PSCs corresponding to Figures 1b and 1c, respectively. We define two key parameters:

(1) V_{ex}, the V_{ph} value at the moment of switching from the "open-circuit" state/operating conditions to the "short-circuit" state (marking the start of short-circuit charge extraction). V_{ex} encompasses contributions from both free charges and ion-trapped charges and can reflect the carrier concentration in the device.

(2) $V_{r\text{-}oc}/V_{r\text{-}app}$, the peak of the voltage recovery signal after returning to the "open-circuit" state. V_r represents the amount of ion accumulation at the interface and can reflect the concentration of ion-captured carriers. This lays the foundation for the quantitative analysis of carrier-ion interactions under actual operating conditions.

Before examining the operating conditions, we undertook a comprehensive study of ion migration in the device while in an "open-circuit" state. We selected the classic $MAPbI_3$ device, as shown in Figure 2a, which achieves an efficiency of 21.31%. The OCVD experiment was conducted first as a foundation for the variable delay mode VL-TPT experiment. As displayed in Figure 2b, two distinct voltage decay processes are observed from the OCVD trace, with a dramatic drop of V_{ph} from the maximum value to ~0.87 V within the first 100 ms and a long-lived tail extending for tens of seconds. The rapid decay process is attributed to the recombination of free charges, while the ultraslow OCVD response observed at long delay times (V_{ph} < 0.87 V) remains a topic of debate. Some attribute it to electrostatic potential relaxation from ionic accumulation,[13,33,34] while others suggest it results from hindered charge transfer due to band bending.[15,35] Despite this uncertainty, we can consider that this part is associated with the recombination of ion-related charges.

Next, we utilized the VL-TPT technique in variable time delay mode to investigate ion migration during the OCVD process (carrier concentration decay process). As illustrated in Figure 2c, at high voltages (V_{ex} > 0.87 V), $V_{r\text{-}oc}$ reaches a stable level

https://doi.org/10.1021/acs.jpclett.4c03068
J. Phys. Chem. Lett. 2024, 15, 11903−11910

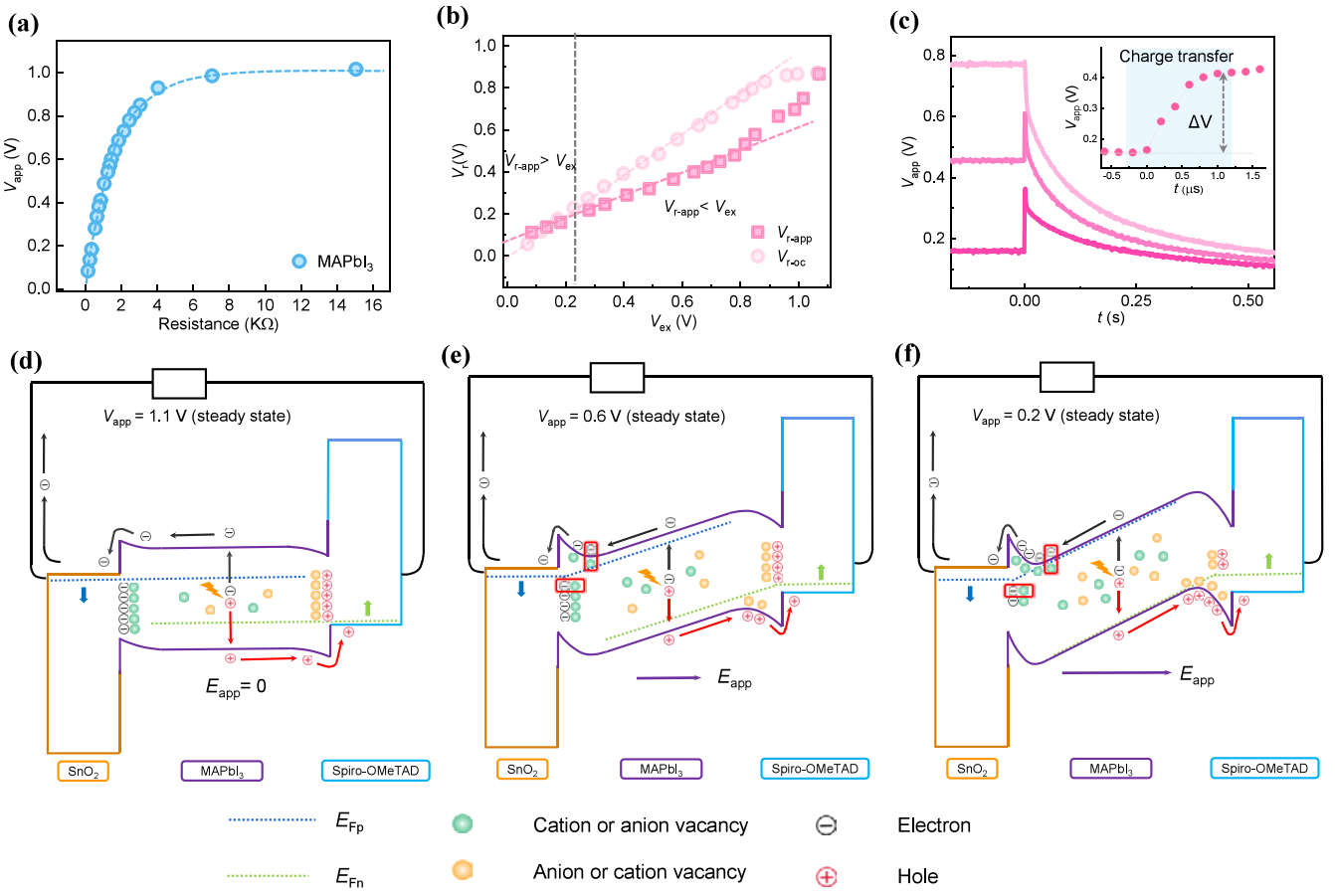

Figure 3. (a) Variation of V_{app} with load for the $MAPbI_3$ device, showing that V_{app} increases with the load and approaches V_{oc} when the load becomes sufficiently large. (b) $V_{r\text{-}app}$ variation as a function of V_{ex} for the $MAPbI_3$ device. $V_{r\text{-}app}$ increases with V_{app} and remains unsaturated. (c) The overshoot voltage curves at different V_{app}. The inset illustrates the microsecond-scale process, where charges trapped in potential wells are released to the transport layers. (d–f) The energy band structure under operating conditions of the $MAPbI_3$ device at applied voltage (V_{app}) values of 1.1 V (panel (d)), 0.6 V (panel (e)), and 0.2 V (panel (f)), respectively. As the load decreases, the working electric field increases, causing the energy bands to tilt and the potential wells to enlarge, which results in a reduction of surface-accumulated ions. (See the text for details.)

($V_{r\text{-}oc,\ max}$ = 0.87 V), indicating that during the rapid recombination of free charges, ions accumulated at the interface under the influence of the photoelectric field remain unmoved, as their migration time scale (ms–s) greatly exceeds that (μs) of charge recombination.[27,28] In contrast, at lower voltages (V_{ex} < 0.87 V), $V_{r\text{-}oc}$ progressively decreases with a reduction in V_{ex}, displaying a slope approximately equal to 1 ($V_{ex} = V_{r\text{-}oc}$). This process demonstrates a direct correlation between the concentration of ion-related carriers and the amount of ions accumulated at the interface. After the recombination of free charges, ions migrate from the interface to the bulk phase, releasing the charges trapped by the ions into the conduction band, leading to recombination. The above conclusions further validate the PITS model, offering insights into the interaction model of ions and carriers under open-circuit conditions.

Under illumination, electrons and holes are transported to the electron transport layer (ETL) and hole transport layer (HTL), respectively, and the splitting of the Fermi level generates a stable photovoltage (V_{ph}). Within the perovskite layer, under the action of the photoelectric field, cations migrate toward the ETL, while anions move toward the HTL.[13,35−37] Ion accumulated at the interfaces traps charges electrostatically, forming polarization-induced trap state and altering the energy band structure, as shown in Figure 2d. When illumination is removed, V_{ph} decays due to charge recombination, and the quasi-Fermi levels (E_{Fn} and E_{Fp}) converge toward the equilibrium Fermi level (E_{F0}). At this point, the ions have not yet moved, and the amount of ions ($V_{r\text{-}oc}$) at the interface remains constant, unaffected by the decrease in carrier concentration (V_{ex}). After the rapid recombination of free charges, ions begin to migrate from the interface back to the bulk, releasing the trapped charges. This portion of the charge returns to the conduction band, subsequently leading to recombination. At this stage, the accumulation of ions ($V_{r\text{-}oc}$) at the interface diminishes as the carrier concentration (V_{ex}) decreases, as depicted in Figures 2e and 2f, showing photovoltage decay to 0.6 and 0.2 V, respectively.

Subsequently, we begin the research on ion migration under operating conditions using the VL-TPT technique at fluctuating load mode. Under a certain load and illumination, the operating voltage of the device gradually rises to a stable value (V_{app}), which is effectively adjusted by changing the load resistance. As shown in Figure 3a, V_{app} increases with the load size until eventually approaching open-circuit photovoltage. Figure S3 shows typical VL-TPT curves for $MAPbI_3$ PSCs with load resistances of 2400 Ω and 800 Ω, respectively. Unlike the varying time delay mode, in this case, the time delay is fixed at zero, thereby V_{ex} is equal to V_{app}, indicating charge extraction is performed while the operating voltage is stable. After multiple sets of VL-TPT experiments under different loads, Figure 3b

https://doi.org/10.1021/acs.jpclett.4c03068
J. Phys. Chem. Lett. 2024, 15, 11903−11910

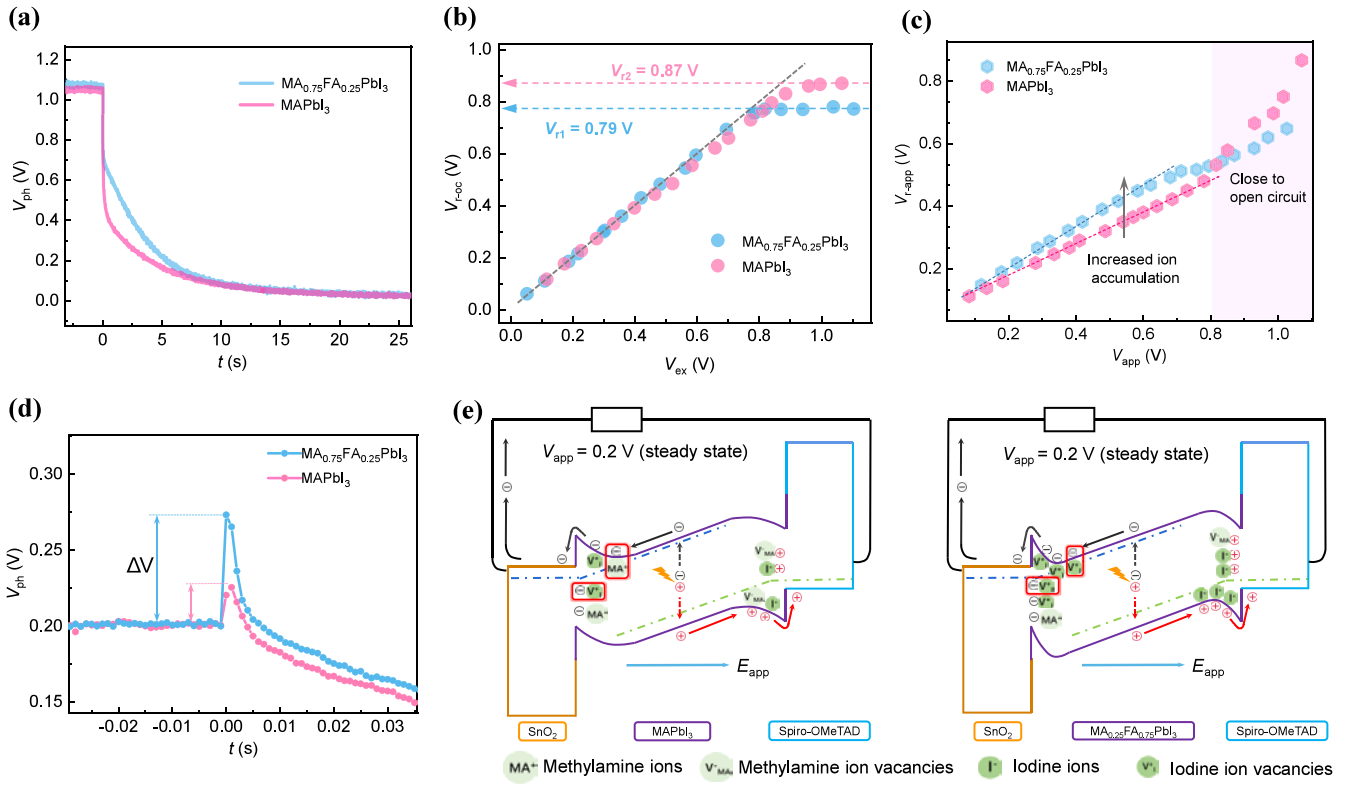

Figure 4. (a) Complete OCVD profiles of the $MAPbI_3$ and $MA_{0.75}FA_{0.25}PbI_3$ devices. (b) $V_{r\text{-}oc}$ variation as a function of V_{ex} for devices, showing saturation voltages of 0.87 V for $MAPbI_3$ and 0.79 V for $MA_{0.75}FA_{0.25}PbI_3$. (c) $V_{r\text{-}app}$ variation as a function of V_{ex} (V_{app}) for devices. (d) The overshoot voltage curves of devices at V_{app} = 0.2 V. (e) Band structures of $MAPbI_3$ and $MA_{0.75}FA_{0.25}PbI_3$ devices with varying potential well sizes.

shows that $V_{r\text{-}app}$ decreases as V_{ex} decreases, indicating that ion accumulation in the device diminishes with a reduction in load. This occurs because the external electric field (E_{app}) generated by the load induces band tilting,[35,38] driving charge transport to the external circuit thereby reducing the carrier concentration within the device. Under the condition that the total amount of photogenerated carriers remains constant, as the load decreases, the increase in E_{app} leads to a reduction in the concentration of residual carriers interacting with ions within the device.

Additionally, the operating voltage output (V_{app} or V_{ex}) is influenced by both free charges and ion-trapped charges, resulting in the relationship V_{ex} (V_{app}) > $V_{r\text{-}app}$, which is straightforward to understand. However, surprisingly, at low V_{ex}, we observe the occurrence of V_{ex} < $V_{r\text{-}app}$. This phenomenon suggests that, under certain small load conditions, some charges within the device are trapped with interfacial ions but do not contribute to the voltage output. The formation of an interfacial potential well occurs when band bending and band tilting simultaneously take place at the interface.[38−40] This potential well is likely the primary reason for this phenomenon, as charges tend to accumulate in the well during transport, allowing for interaction with interfacial ions. The operating voltage overshoot experiment further confirms the above speculation. As shown in Figure 3c, when both the illumination and load are removed, a sharp voltage spike occurs as the device stabilizes at its V_{app}. Many researchers have conducted theoretical and experimental studies on the phenomenon of voltage overshoot, indicating that it results from the transfer of charges that were previously trapped in the potential well to the HTL/ETL.[41−44] The insert of Figure 3c shows that this process occurs at a subtle scale, precisely aligning with the time scale of charge transfer. In addition, the magnitude of the voltage overshoot increases as V_{app} decreases, indicating that the potential wells can store more charges at a lower load. For example, as shown in Figure 3b, when V_{ex} is at 0.1 V, ion accumulation under operating conditions ($V_{r\text{-}app}$) can exceed that in the "open-circuit" state ($V_{r\text{-}oc}$).

Based on the above analysis, we can establish an ion-carrier interactions model under operating conditions. After the device is illuminated, photogenerated carriers are generated within it. Meanwhile, the load connected across the terminals of the device creates E_{app} directed from the ETL to the HTL. which drives charge transport to the external circuit. The remaining charges within the device cause the Fermi level to split, resulting in a stable V_{app}. When the load is sufficiently high, the system approaches open circuit conditions, under the influence of the photoelectric field, with cations accumulating in ETL and anions HTL, forming a polarization-induced trap state as shown in Figure 3d. As the load decreases, the E_{app} strengthens, causing a reduction in the concentration of carriers polarized with the ions at the interface, ultimately resulting in both cations and anions gradually migrating toward the bulk phase. Consequently, the accumulation of interfacial ions decreases as the load diminishes, as illustrated in Figures 3d−f, with examples provided at V_{app} = 1.1, 0.6, and 0.2 V, respectively. At the same time, the accumulation of ions at the interface induces band bending, and as the bands tilt, an interfacial potential well is established. A fraction of the charges become trapped within this potential well, forming polarization-induced trap states with the ions, thereby augmenting the relative concentration of interfacial ions. This accumulation effect of the potential well on the charges is particularly pronounced under conditions of relatively low load. The E_{app} and the potential well significantly alter the mechanism

https://doi.org/10.1021/acs.jpclett.4c03068
J. Phys. Chem. Lett. 2024, 15, 11903−11910

of ion-carrier interactions under operating conditions compared to open-circuit conditions.

FA^+ is frequently employed for compositional optimization and can suppress ion migration,[45,46] thus we also conducted experiments on $MA_{0.75}FA_{0.25}PbI_3$ devices. The basic characterization of the devices is provided in Figures S4−S8. First, under open-circuit conditions, as shown in Figure 4a, devices exhibit similar OCVD curve trends, each showing two distinct photovoltage decay processes. Notably, the $MA_{0.75}FA_{0.25}PbI_3$ device exhibits slower voltage decay. The spatial steric effect of FA^+ effectively slows down the ion migration rate,[47,48] leading to an impediment in the recombination of ion-related charges. Figure 4b further quantifies this, showing $V_{r,max}$ of 0.87 V for $MAPbI_3$ and 0.79 V for $MA_{0.75}FA_{0.25}PbI_3$, respectively, indicating that fewer ions accumulate at the interface in the $MA_{0.75}FA_{0.25}PbI_3$ device. Thus, introducing a moderate amount of FA^+ slows ion migration and reduces interfacial ion accumulation.

Next, we investigate the ion migration behavior of the two devices under operating conditions. As shown in Figure 4c, the $V_{r\text{-}app}-V_{app}$ curves reveal that, except when close to an open circuit (at high V_{ex}), the $V_{r\text{-}app}$ of $MA_{0.75}FA_{0.25}PbI_3$ is lower than that of $MAPbI_3$. In most cases, when V_{ex} is equal, the $V_{r\text{-}app}$ of $MA_{0.75}FA_{0.25}PbI_3$ is greater than that of $MAPbI_3$. This indicates that when the devices output the same power, $MA_{0.75}FA_{0.25}PbI_3$ accumulates more ions at the interface during operation. Evidently, under operating conditions, FA^+ accelerates ion accumulation at the device interfaces. Based on the ion migration model for operation conditions, this effect is most likely due to the influence of potential wells. To verify this hypothesis, we performed a voltage overshoot experiment on both devices for comparison. As shown in Figure 4d, at V_{app} of 0.2 V, the $MA_{0.75}FA_{0.25}PbI_3$ increases the overshoot voltage, suggesting that the $MA_{0.75}FA_{0.25}PbI_3$ device experiences greater charge accumulation in the potential wells, interacting more with the ions, as depicted in Figure 4e.

Generally, FA^+ regulates the types of mobile ions, altering the migration dynamics within the device. As shown in Figure S9, the open-circuit voltage build-up (OCVB) measurements reveal a slower photovoltage rise on the millisecond time scale for the $MA_{0.75}FA_{0.25}PbI_3$ device,[49] indicating FA^+ significantly inhibits cation migration. Therefore, we hypothesize that the reason for the greater accumulation of ions in the $MA_{0.75}FA_{0.25}PbI_3$ device under operating conditions is that the increased proportion of easily migratory iodide ions and vacancies enhances doping near the transport layers,[44] leading to more pronounced band bending and charge accumulation. In addition, our findings provide valuable insights for improving the devices' long-term stability. By understanding the time scales and mechanisms of ion migration, we can further optimize the material components to reduce ion-related degradation, which is crucial for enhancing long-term stability.

In summary, this study employs a customized variable load transient photovoltaic technique (VL-TPT) to investigate the ion migration mechanisms in PSCs under operating conditions. Experimental results indicate a significant direct correlation between the concentration of photogenerated carriers and ion accumulation under open-circuit conditions. Under actual operating conditions, the amount of ion accumulation decreases as the load is reduced. This phenomenon is because the charge is derived from transport to the external circuit, thereby lowering the carrier concentration within the device. Furthermore, the observed abnormal increase in interface ions under low-load conditions arises from the interaction between charges accumulated in the interface potential well during the transport process and ions. Studies on the $MA_{0.75}FA_{0.25}PbI_3$ device further reveal that the introduction of FA^+ effectively suppresses ion migration in the open-circuit state but accelerates interface ion accumulation during operating conditions. This study provides a comprehensive analysis of ion migration under realistic operating conditions, offering valuable insights for optimizing device composition and enhancing long-term stability.

■ ASSOCIATED CONTENT

Supporting Information

The Supporting Information is available free of charge at https://pubs.acs.org/doi/10.1021/acs.jpclett.4c03068.

Experimental section, a detailed explanation of the PITS model, and fundamental characterization data such as OCVB curves, PL spectra, and XRD patterns (PDF)

■ AUTHOR INFORMATION

Corresponding Authors

Meicheng Li − *State Key Laboratory of Alternate Electrical Power System with Renewable Energy Sources, North China Electric Power University, Beijing 102206, China*; Email: mcli@ncepu.edu.cn

Xicheng Ai − *Key Laboratory of Advanced Light Conversion Materials and Biophotonics, Department of Chemistry, Renmin University of China, Beijing 100872, China*; orcid.org/0000-0002-3539-3946; Email: xcai@ruc.edu.cn

Authors

Yiyi Li − *Key Laboratory of Advanced Light Conversion Materials and Biophotonics, Department of Chemistry, Renmin University of China, Beijing 100872, China*; orcid.org/0009-0005-5823-0030

Shujie Qu − *State Key Laboratory of Alternate Electrical Power System with Renewable Energy Sources, North China Electric Power University, Beijing 102206, China*

Jiyuan Wu − *Key Laboratory of Advanced Light Conversion Materials and Biophotonics, Department of Chemistry, Renmin University of China, Beijing 100872, China*

Haohui Fang − *Key Laboratory of Advanced Light Conversion Materials and Biophotonics, Department of Chemistry, Renmin University of China, Beijing 100872, China*

Ning Liu − *Key Laboratory of Advanced Light Conversion Materials and Biophotonics, Department of Chemistry, Renmin University of China, Beijing 100872, China*

Peng Cui − *State Key Laboratory of Alternate Electrical Power System with Renewable Energy Sources, North China Electric Power University, Beijing 102206, China*

Complete contact information is available at: https://pubs.acs.org/10.1021/acs.jpclett.4c03068

Author Contributions

▽Authors Y. Li and S. Qu contributed equally to this work.

Notes

The authors declare no competing financial interest.

■ ACKNOWLEDGMENTS

We gratefully acknowledge funding from the National Natural Science Foundation of China (NSFC) (Grant No. 22273119), and this work was supported by the Outstanding Innovative

Talents Cultivation Funded Programs 2023 of Renmin University of China.

REFERENCES

(1) Kojima, A.; Teshima, K.; Shirai, Y.; Miyasaka, T. Organometal Halide Perovskites as Visible-Light Sensitizers for Photovoltaic Cells. *J. Am. Chem. Soc.* **2009**, *131*, 6050−6051.

(2) Green, M. A.; Dunlop, E. D.; Yoshita, M.; Kopidakis, N.; Bothe, K.; Siefer, G.; Hinken, D.; Rauer, M.; Hohl-Ebinger, J.; Hao, X. Solar Cell Efficiency Tables (Version 64). *Prog. Photovoltaics* **2024**, *32*, 425−441.

(3) Stranks, S. D.; Eperon, G. E.; Grancini, G.; Menelaou, C.; Alcocer, M. J. P.; Leijtens, T.; Herz, L. M.; Petrozza, A.; Snaith, H. J. Electron-Hole Diffusion Lengths Exceeding 1 Micrometer in an Organometal Trihalide Perovskite Absorber. *Science* **2013**, *342*, 341−344.

(4) Jeon, N. J.; Noh, J. H.; Yang, W. S.; Kim, Y. C.; Ryu, S.; Seo, J.; Seok, S. I. Compositional Engineering of Perovskite Materials for High-Performance Solar Cells. *Nature* **2015**, *517*, 476−480.

(5) Miyata, A.; Mitioglu, A.; Plochocka, P.; Portugall, O.; Wang, J. T.-W.; Stranks, S. D.; Snaith, H. J.; Nicholas, R. J. Direct Measurement of the Exciton Binding Energy and Effective Masses for Charge Carriers in Organic−Inorganic Tri-Halide Perovskites. *Nat. Phys.* **2015**, *11*, 582−587.

(6) Balaguera, E. H.; Bisquert, J. Accelerating the Assessment of Hysteresis in Perovskite Solar Cells. *ACS Energy Lett.* **2024**, *9*, 478−486.

(7) Miyano, K.; Yanagida, M.; Tripathi, N.; Shirai, Y. Hysteresis, Stability, and Ion Migration in Lead Halide Perovskite Photovoltaics. *J. Phys. Chem. Lett.* **2016**, *7*, 2240−2245.

(8) Tai, Q.; You, P.; Sang, H.; Liu, Z.; Hu, C.; Chan, H. L.; Yan, F. Efficient and Stable Perovskite Solar Cells Prepared in Ambient Air Irrespective of the Humidity. *Nat. Commun.* **2016**, *7*, 11105.

(9) Pavlovetc, I. M.; Brennan, M. C.; Draguta, S.; Ruth, A.; Moot, T.; Christians, J. A.; Aleshire, K.; Harvey, S. P.; Toso, S.; Nanayakkara, S. U.; Messinger, J.; Luther, J. M.; Kuno, M. Suppressing Cation Migration in Triple-Cation Lead Halide Perovskites. *ACS Energy Lett.* **2020**, *5*, 2802−2810.

(10) Kayesh, M. E.; Karim, M. A.; He, Y.; Shirai, Y.; Yanagida, M.; Islam, A. Minimization of Energy Level Mismatch of PCBM and Surface Passivation for Highly Stable Sn-Based Perovskite Solar Cells by Doping n-Type Polymer. *Small* **2024**, *20*, e2402896.

(11) Imran, T.; Aziz, H. S.; Iftikhar, T.; Ahmad, M.; Xie, H.; Su, Z.; Yan, P.; Liu, Z.; Liang, G.; Chen, W.; Chen, S. Interfacial Band Bending and Suppressing Deep Level Defects via Eu-MOF-Mediated Cathode Buffer Layer in an MA-Free Inverted Perovskite Solar Cell with High Fill Factor. *Energy Environ. Sci.* **2024**, *17*, 7234−7246.

(12) Sun, X.; Li, Y.; Liu, D.; Liu, R.; Zhang, B.; Tian, Q.; Fan, B.; Wang, X.; Li, Z.; Shao, Z.; Wang, X.; Cui, G.; Pang, S. V_{OC} of Inverted Perovskite Solar Cells Based on N-Doped PCBM Exceeds 1.2 V: Interface Energy Alignment and Synergistic Passivation. *Adv. Energy Mater.* **2023**, *13*, No. 2302191.

(13) Gottesman, R.; Lopez-Varo, P.; Gouda, L.; Jimenez-Tejada, J. A.; Hu, J.; Tirosh, S.; Zaban, A.; Bisquert, J. Dynamic Phenomena at Perovskite/Electron-Selective Contact Interface as Interpreted from Photovoltage Decays. *Chem.* **2016**, *1*, 776−789.

(14) Hu, J.; Gottesman, R.; Gouda, L.; Kama, A.; Priel, M.; Tirosh, S.; Bisquert, J.; Zaban, A. Photovoltage Behavior in Perovskite Solar Cells under Light-Soaking Showing Photoinduced Interfacial Changes. *ACS Energy Lett.* **2017**, *2*, 950−956.

(15) Pockett, A.; Carnie, M. J. Ionic Influences on Recombination in Perovskite Solar Cells. *ACS Energy Lett.* **2017**, *2*, 1683−1689.

(16) Lopez-Varo, P.; Jiménez-Tejada, J. A.; García-Rosell, M.; Anta, J. A.; Ravishankar, S.; Bou, A.; Bisquert, J. Effects of Ion Distributions on Charge Collection in Perovskite Solar Cells. *ACS Energy Lett.* **2017**, *2*, 1450−1453.

(17) Krückemeier, L.; Liu, Z.; Kirchartz, T.; Rau, U. Quantifying Charge Extraction and Recombination Using the Rise and Decay of the Transient Photovoltage of Perovskite Solar Cells. *Adv. Mater.* **2023**, *35*, No. 2300872.

(18) Ravishankar, S.; Kruppa, L.; Jenatsch, S.; Yan, G.; Wang, Y. Discerning Rise Time Constants to Quantify Charge Carrier Extraction in Perovskite Solar Cells. *Energy Environ. Sci.* **2024**, *17*, 1229−1243.

(19) Huang, K.; Feng, X.; Li, H.; Long, C.; Liu, B.; Shi, J.; Meng, Q.; Weber, K.; Duong, T.; Yang, J. Manipulating the Migration of Iodine Ions via Reverse-Biasing for Boosting Photovoltaic Performance of Perovskite Solar Cells. *Adv. Sci.* **2022**, *9*, No. e2204163.

(20) Kim, M.-c.; Ahn, N.; Cheng, D.; Xu, M.; Ham, S.-Y.; Pan, X.; Kim, S. J.; Luo, Y.; Fenning, D. P.; Tan, D. H. S.; Zhang, M.; Zhu, G.; Jeong, K.; Choi, M.; Meng, Y. S. Imaging Real-Time Amorphization of Hybrid Perovskite Solar Cells under Electrical Biasing. *ACS Energy Lett.* **2021**, *6*, 3530−3537.

(21) Wu, X.; Ma, J.; Qin, M.; Guo, X.; Li, Y.; Qin, Z.; Xu, J.; Lu, X. Control over Light Soaking Effect in All-Inorganic Perovskite Solar Cells. *Adv. Funct. Mater.* **2021**, *31*, No. 2101287.

(22) Ahmadi, M.; Muckley, E. S.; Ivanov, I. N.; Lorenz, M.; Li, X.; Ovchinnikova, O.; Lukosi, E. D.; Tisdale, J. T.; Blount, E.; Kravchenko, I. I.; Kalinin, S. V.; Hu, B.; Collins, L. Environmental Gating and Galvanic Effects in Single Crystals of Organic-Inorganic Halide Perovskites. *ACS Appl. Mater. Interfaces* **2019**, *11*, 14722−14733.

(23) Liu, Y.; Ievlev, A. V.; Borodinov, N.; Lorenz, M.; Xiao, K.; Ahmadi, M.; Hu, B.; Kalinin, S. V.; Ovchinnikova, O. S. Direct Observation of Photoinduced Ion Migration in Lead Halide Perovskites. *Adv. Funct. Mater.* **2021**, *31*, No. 2008777.

(24) Li, C.; Guerrero, A.; Huettner, S.; Bisquert, J. Unravelling the Role of Vacancies in Lead Halide Perovskite through Electrical Switching of Photoluminescence. *Nat. Commun.* **2018**, *9*, 5113.

(25) Peng, W.; Aranda, C.; Bakr, O. M.; Garcia-Belmonte, G.; Bisquert, J.; Guerrero, A. Quantification of Ionic Diffusion in Lead Halide Perovskite Single Crystals. *ACS Energy Lett.* **2018**, *3*, 1477−1481.

(26) Kim, H.-S.; Jang, I.-H.; Ahn, N.; Choi, M.; Guerrero, A.; Bisquert, J.; Park, N.-G. Control of I-V Hysteresis in $CH_3NH_3PbI_3$ Perovskite Solar Cell. *J. Phys. Chem. Lett.* **2015**, *6*, 4633−4639.

(27) Futscher, M. H.; Lee, J. M.; McGovern, L.; Muscarella, L. A.; Wang, T. Y.; Haider, M. I.; Fakharuddin, A.; Schmidt-Mende, L.; Ehrler, B. Quantification of Ion Migration in $CH_3NH_3PbI_3$ Perovskite Solar Cells by Transient Capacitance Measurements. *Mater. Horizons* **2019**, *6*, 1497−1503.

(28) Bag, M.; Renna, L. A.; Adhikari, R. Y.; Karak, S.; Liu, F.; Lahti, P. M.; Russell, T. P.; Tuominen, M. T.; Venkataraman, D. Kinetics of Ion Transport in Perovskite Active Layers and Its Implications for Active Layer Stability. *J. Am. Chem. Soc.* **2015**, *137*, 13130−13137.

(29) Yuan, S.; Wang, H.-Y.; Lou, F.; Wang, X.; Wang, Y.; Qin, Y.; Ai, X.-C.; Zhang, J.-P. Polarization-Induced Trap States in Perovskite Solar Cells Revealed by Circuit-Switched Transient Photoelectric Technique. *J. Phys. Chem. C* **2022**, *126*, 3696−3704.

(30) Qu, S.; Huang, H.; Wang, J.; Cui, P.; Li, Y.; Wang, M.; Li, L.; Yang, F.; Sun, C.; Zhang, Q.; Zhu, P.; Wang, Y.; Li, M. Revealing and Inhibiting the Facet-related Ion Migration for Efficient and Stable Perovskite Solar Cells. *Angew. Chem., Int. Ed.* **2024**, No. e202415949.

(31) Sandeep, P.; Bisht, P. B. Effect of Adsorbed Concentration on the Radiative Rate Enhancement of Photoexcited Molecules Embedded in Single Microspheres. *J. Chem. Phys.* **2005**, *123*, No. 204713.

(32) Yuan, S.; Lou, F.; Li, Y.; Wang, H.-Y.; Wang, Y.; Ai, X.-C.; Zhang, J.-P. Targeted Suppression of Hysteresis Effect in Perovskite Solar Cells Through the Inhibition of Cation Migration. *Appl. Phys. Lett.* **2023**, *122*, No. 133502.

(33) Pockett, A.; Eperon, G. E.; Sakai, N.; Snaith, H. J.; Peter, L. M.; Cameron, P. J. Microseconds, milliseconds and seconds: deconvoluting the dynamic behaviour of planar perovskite solar cells. *Phys. Chem. Chem. Phys.* **2017**, *19*, 5959−5970.

(34) Bertoluzzi, L.; Sanchez, R. S.; Liu, L.; Lee, J.-W.; Mas-Marza, E.; Han, H.; Park, N.-G.; Mora-Sero, I.; Bisquert, J. Cooperative Kinetics of Depolarization in $CH_3NH_3PbI_3$ Perovskite Solar Cells. *Energy Environ. Sci.* **2015**, *8*, 910−915.

(35) Zheng, F.; Wen, X.; Bu, T.; Chen, S.; Yang, J.; Chen, W.; Huang, F.; Cheng, Y.; Jia, B. Slow Response of Carrier Dynamics in Perovskite

https://doi.org/10.1021/acs.jpclett.4c03068
J. Phys. Chem. Lett. 2024, 15, 11903−11910

Interface upon Illumination. *ACS Appl. Mater. Interfaces* **2018**, *10*, 31452−31461.
(36) Shih, Y. C.; Wang, L.; Hsieh, H. C.; Lin, K. F. Effect of Fullerene Passivation on the Charging and Discharging Behavior of Perovskite Solar Cells: Reduction of Bound Charges and Ion Accumulation. *ACS Appl. Mater. Interfaces* **2018**, *10*, 11722−11731.
(37) Ebadi, F.; Aryanpour, M.; Mohammadpour, R.; Taghavinia, N. Coupled Ionic-Electronic Equivalent Circuit to Describe Asymmetric Rise and Decay of Photovoltage Profile in Perovskite Solar Cells. *Sci. Rep.* **2019**, *9*, 11962.
(38) Chen, Y.; Zhou, W.; Chen, X.; Zhang, X.; Gao, H.; Ouedraogo, N. A. N.; Zheng, Z.; Han, C. B.; Zhang, Y.; Yan, H. In Situ Management of Ions Migration to Control Hysteresis Effect for Planar Heterojunction Perovskite Solar Cells. *Adv. Funct. Mater.* **2022**, *32*, No. 2108417.
(39) Calado, P.; Telford, A. M.; Bryant, D.; Li, X.; Nelson, J.; O'Regan, B. C.; Barnes, P. R. Evidence for Ion Migration in Hybrid Perovskite Solar Cells with Minimal Hysteresis. *Nat. Commun.* **2016**, *7*, 13831.
(40) Belisle, R. A.; Nguyen, W. H.; Bowring, A. R.; Calado, P.; Li, X.; Irvine, S. J. C.; McGehee, M. D.; Barnes, P. R. F.; O'Regan, B. C. Interpretation of Inverted Photocurrent Transients in Organic Lead Halide Perovskite Solar Cells: Proof of the Field Screening by Mobile Ions and Determination of the Space Charge Layer Widths. *Energy Environ. Sci.* **2017**, *10*, 192−204.
(41) Wu, Y.; Shen, H.; Walter, D.; Jacobs, D.; Duong, T.; Peng, J.; Jiang, L.; Cheng, Y. B.; Weber, K. On the Origin of Hysteresis in Perovskite Solar Cells. *Adv. Funct. Mater.* **2016**, *26*, 6807−6813.
(42) Li, L.; Jia, P.; Bi, W.; Tang, Y.; Song, B.; Qin, L.; Lou, Z.; Hu, Y.; Teng, F.; Hou, Y. Impacts of Carrier Trapping and Ion Migration on Charge Transport of Perovskite Solar Cells with TiO_x Electron Transport Layer. *RSC Adv.* **2020**, *10*, 28083−28089.
(43) Tress, W.; Marinova, N.; Moehl, T.; Zakeeruddin, S. M.; Nazeeruddin, M. K.; Grätzel, M. Understanding the Rate-Dependent J−V Hysteresis, Slow Time Component, and Aging in $CH_3NH_3PbI_3$ Perovskite Solar Cells: The Role of a Compensated Electric Field. *Energy Environ. Sci.* **2015**, *8*, 995−1004.
(44) Herterich, J.; Unmüssig, M.; Wagner, L.; Loukeris, G.; Faisst, J.; List, M.; Kohlstädt, M.; Würfel, U. Decoupling of Implied and External V_{OC} Due to Ionic Movement Explaining Transient V_{OC} Overshoot in Perovskite Solar Cells. *Energy Technol.* **2022**, *10*, No. 2100868.
(45) Li, Z.; Yang, M.; Park, J.-S.; Wei, S.-H.; Berry, J. J.; Zhu, K. Stabilizing Perovskite Structures by Tuning Tolerance Factor: Formation of Formamidinium and Cesium Lead Iodide Solid-State Alloys. *Chem. Mater.* **2016**, *28*, 284−292.
(46) Liu, Z.; Liu, P.; Li, M.; He, T.; Liu, T.; Yu, L.; Yuan, M. Efficient and Stable FA-Rich Perovskite Photovoltaics: From Material Properties to Device Optimization. *Adv. Energy Mater.* **2022**, *12*, No. 2200111.
(47) Oranskaia, A.; Yin, J.; Bakr, O. M.; Brédas, J.-L.; Mohammed, O. F. Halogen Migration in Hybrid Perovskites: The Organic Cation Matters. *J. Phys. Chem. Lett.* **2018**, *9*, 5474−5480.
(48) Zhang, T.; Meng, X.; Bai, Y.; Xiao, S.; Hu, C.; Yang, Y.; Chen, H.; Yang, S. Profiling the Organic Cation-Dependent Degradation of Organolead Halide Perovskite Solar Cells. *J. Mater. Chem. A* **2017**, *5*, 1103−1111.
(49) Lou, F.; Yuan, S.; Wang, X.; Wang, H.-Y.; Wang, Y.; Qin, Y.; Ai, X.-C.; Zhang, J.-P. Distinguishing the Migration Time Scale of Ion Species in Perovskite Solar Cells. *Chem. Phys. Lett.* **2022**, *796*, No. 139570.

https://doi.org/10.1021/acs.jpclett.4c03068
J. Phys. Chem. Lett. 2024, 15, 11903−11910